RSC Advances

PAPER

View Article Online
View Journal | View Issue



Cite this: *RSC Adv.*, 2020, **10**, 26142

# Magnetic core–shell $Fe_3O_4$@$Cu_2O$ and $Fe_3O_4$@$Cu_2O$–Cu materials as catalysts for aerobic oxidation of benzylic alcohols assisted by TEMPO and *N*-methylimidazole†

Binyu Xu,[a] Samuthirarajan Senthilkumar,[b] Wei Zhong,*[b] Zhongquan Shen,[b] Chunxin Lu[b] and Xiaoming Liu *[ab]

In this work, core–shell $Fe_3O_4$@$Cu_2O$ and $Fe_3O_4$@$Cu_2O$–Cu nanomaterials for aerobic oxidation of benzylic alcohols are reported with 2,2,6,6-tetramethylpiperidine-*N*-oxyl (TEMPO) and *N*-methylimidazole (NMI) as the co-catalysts. To anchor $Cu_2O$ nanoparticles around the magnetic particles under solvothermal conditions, the magnetic material $Fe_3O_4$ was modified by grafting a layer of L-lysine (L-Lys) to introduce $-NH_2$ groups at the surface of the magnetic particles. With amine groups as the anchor, $Cu(NO_3)_2$ was used to co-precipitate the desired $Cu_2O$ by using ethylene glycol as the reducing agent. Prolonging the reaction time would lead to over-reduced forms of the magnetic materials in the presence of copper, $Fe_3O_4$@$Cu_2O$–Cu. The nanomaterials and its precursors were fully characterized by a variety of spectroscopic techniques. In combination with both TEMPO and NMI, these materials showed excellent catalytic activities in aerobic oxidation of benzylic alcohols under ambient conditions. For most of the benzylic alcohols, the conversion into aldehydes was nearly quantitative with aldehydes as the sole product. The materials were recyclable and robust. Up to 7 repeat runs, its activity dropped less than 10%. The over-reduced materials, $Fe_3O_4$@$Cu_2O$–Cu, exhibited slightly better performance in durability. The magnetic properties allowed easy separation after reaction by simply applying an external magnet.

Received 6th May 2020
Accepted 2nd July 2020

DOI: 10.1039/d0ra04064a

rsc.li/rsc-advances



## 1. Introduction

The selective oxidation of alcohols to aldehydes is an important organic transformation in the pharmaceutical industry as well as in other organic synthesis.[1] Of the aldehydes, aromatic aldehydes are often used for the synthesis of drugs, vitamins, dyes, spices, and resins and so on.[2] To date, many homogeneous as well as heterogeneous catalysts have been developed for the oxidation of alcohols to prepare aldehydes or ketones.[3–7] Despite the progress achieved so far, the research in this area remains intensive due to existing challenges in this conversion such as harsh conditions, expensive metals, reusability of the catalysts. In nature, copper-based catalysis plays vital roles in biological systems.[8] One of the examples is the copper-containing enzyme, galactose oxidase (GOase), which catalyses the aerobic oxidation of primary alcohols in some species of fungi under physiological conditions.[9] Tremendous efforts have been taken to mimic the enzyme in both approaches, structurally and functionally mimicking based on various copper complexes.[10–12] Homogeneous system reported by Semmelhack[13] *et al.*, Cu(I)/TEMPO (2,2,6,6-tetramethyl-1-piperidine-*N*-oxyl), contributed significantly to this copper-based catalysis. Later on, Sheldon[14] *et al.*, Stahl and co-workers[15–17] and other research groups reported a wide range of homogeneous copper catalysts which were based on the combination of various nitroxyl radicals and ligands for the oxidation of various alcohols.[18–20] Some of the catalytic systems showed promising catalytic activity in aerobic oxidation of alcohols including aliphatic alcohols.[21,22] One such example was $Cu^I$/TEMPO/NMI system which could effectively catalyse the aerobic oxidation of 1-octanol.[23] However, there have been disadvantages for these systems one way or another, for example, tedious synthesis when specific ligand is needed, problems in catalyst recovery and reusability. To address these issues, a variety of heterogeneous catalysts supported on matrices have been developed. A wide range of materials such as clay, zeolite, metal organic frameworks, polymers, activated carbon, silicates, magnetic materials *etc.*, have been employed as such a matrix.[24,25]

[a]*School of Chemistry, Nanchang University, Nanchang, Jiangxi, China. E-mail: xiaoming.liu@mail.zjxu.edu.cn*

[b]*College of Biological, Chemical Sciences and Engineering, Jiaxing University, Jiaxing, Zhejiang, China. E-mail: weizhong@mail.zjxu.edu.cn*

† Electronic supplementary information (ESI) available: Synthesis and characterization details for the materials and TEMPOH. See DOI: 10.1039/d0ra04064a

About two decades ago, a pioneering work by Ley *et al.* demonstrated a polymer-supported perruthenate for the aerobic oxidation of alcohols.[26] Further, they found that mesoporous silicate (MCM-41) could be an alternative support for the catalyst.[27] Polyoxometalates was also turned out a good carrier to support palladium nanocatalyst for the aerobic oxidation of secondary alcohols in aqueous medium and the catalyst was recoverable.[28] Polystyrene was reported as a matrix to support gold–platinum nanoparticles for the aerobic oxidation of 1-phenylethanol under mild conditions.[29] Although the noble metal catalysts such as Ru, Pt, Pd and Au supported on matrices showed excellent efficiency and selectivity for this aerobic oxidation,[30] it is desirable to develop non-noble metal catalysts in terms of both cost and sustainability. Recent developments in this regard have suggested that employing non-precious metals to assemble catalytic systems is possible. For example, copper could be supported on MOF for aerobic oxidation of alcohols under various conditions.[31,32] Montmorillonite was also used to support mettaloporphyrins (Co, Fe, Mn) for efficient catalysis on the oxidation of both aromatic and aliphatic alcohols.[33]

Transition metal oxides, on one hand, could be the matrix to support catalysts. On the other hand, the metal sites of the oxides could be promising catalysts with adjustable electronic structures widely used in various organic transformations involving electron transfer reactions.[34,35] Albadi *et al.* reported the first row transition-metals and its oxides that could be able to oxidize alcohols in presence of molecular oxygen under reflux conditions.[36] For example, copper, the active site in galactose oxidase catalysing aerobic oxidation of primary alcohols into aldehydes, was employed in a number of heterogeneous catalysts such as Au–CuO,[37] CuO–rectorite,[38] Cu–$MnO_x$[39] and Cu–$TiO_2$ (ref. 40) which catalysed effectively the selective oxidation of benzyl alcohols into aldehydes.

In viewing of the low cost of copper and its biological relevance, cuprous oxide combining with its magnetisation was considered to further to be exploited in heterogeneity as heterogeneous catalysts. Of the many magnetic materials,[41–44] $Fe_3O_4$ is the most favourable option due to easy functionalization and low cost. Grafting a layer of organic modifiers or inorganic linkers such as polymers, organosilanes, aminoacids *etc.*, onto its surface would help to protect the magnetite and allow easy access for the coordination of metal catalysts.[45–47] $Fe_3O_4$@$Cu_2O$ showed photocatalytic activity in degradation of organic dyes as well as the synthesis of quinazolines.[48,49] However, to our best knowledge, the employment of such system in aerobic oxidation of alcohols into aldehydes have not been reported. Being inspired by the copper chemistry on aerobic oxidation of alcohols in biology and the easy recovery property of the $Fe_3O_4$-based cuprous oxide, herein, we report the preparation of $Fe_3O_4$@$Cu_2O$ as well as its over-reduced form, $Fe_3O_4$@$Cu_2O$–Cu, their characterisations and catalytic activity on selective aerobic oxidation of benzylic alcohols into benzylic aldehydes. With the presence of TEMPO and *N*-methylimidazole (NMI), the materials could oxidise nearly quantitatively most of the benzylic alcohols examined in this work into corresponding aldehydes at ambient temperature. The two materials exhibited easy separation and robustness. The loss in converting yields for two materials were less than 10% up to 7 runs with the over-reduced catalyst showing slightly better durability.

## 2. Results and discussion

### 2.1 Preparation and characterization of the nanomaterials

The preparation of core–shell nanomaterials is illustrated in Scheme 1. First, $Fe_3O_4$ nanoparticles with hydroxyl groups on their surfaces were grafted with L-Lys to introduce $-NH_2$ groups that were used as anchors for the immobilization of the *in situ* formed $Cu_2O$ nanoparticles. The formation of materials of $Fe_3O_4$, $Fe_3O_4$-L-Lys and $Fe_3O_4$-L-Lys@$Cu_2O$ were stepwise confirmed using FTIR spectroscopy as shown in Fig. 1. The presence of hydroxyl groups on the surface of magnetite ($Fe_3O_4$) was evidenced by the strong absorption peak at 3423 $cm^{-1}$ and a sharp peak at 616 $cm^{-1}$ corresponding to the stretching vibration of Fe–O bond as shown in Fig. 1b. The L-lysine modified $Fe_3O_4$ was proved by the presence of a sharp peak at 1619 $cm^{-1}$ ($COO^-$), and a broad peak at 3435 ($NH_2$) and 607 $cm^{-1}$ (Fe–O), respectively, as shown in Fig. 2c. Finally, the *in situ* formed $Cu_2O$ on the surface of L-lysine modified $Fe_3O_4$ was confirmed by the presence of an additional sharp peak at 629 $cm^{-1}$ which is assigned to the stretching vibrations of Cu–O as shown in Fig. 2d. These results suggested that the *in situ* formed $Cu_2O$ was successfully anchored to the surface of the magnetic particles through the coordinating interaction of the L-lysine with copper. EDX analysis showed additional evidence for the presence of Fe, Cu, N, C, O in the core–shell $Fe_3O_4$@$Cu_2O$ nanomaterials and the weight of copper present in the catalyst was about 49%, equivalent to 3.8 : 1 in molar ratio for Cu : Fe (Table S1†).

The powder XRD patterns of the as prepared $Fe_3O_4$@$Cu_2O$/$Fe_3O_4$@$Cu_2O$–Cu and the magnetic precursors are shown in Fig. 2. The observed peaks for the formation of $Cu_2O$@$Fe_3O_4$ nanomaterials at 4 h are clearly matched with the PDF Card No. 19-0629 of $Fe_3O_4$ and PDF Card No. 05-0667 of $Cu_2O$ nanoparticles, respectively. Furthermore, no other peaks are observed around 20°, indicating that the products were purely face-centred cubic $Fe_3O_4$ crystalline phase. Prolonging the reaction time produced the over-reduced materials $Fe_3O_4$@$Cu_2O$–Cu and $Fe_3O_4$@Cu, as indicated by the additional three

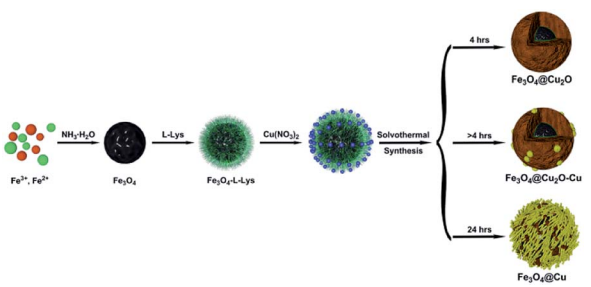


Scheme 1 Synthetic route for the preparation of core–shell nanomaterials.

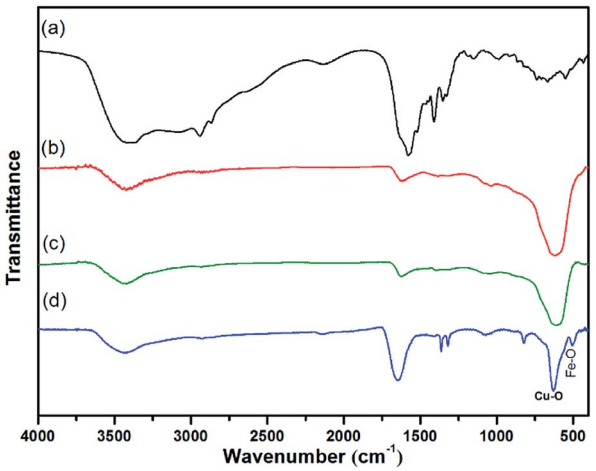


Fig. 1 FT-IR spectra of (a) L-Lys, (b) $Fe_3O_4$, (c) $Fe_3O_4$–L-Lys and (d) $Fe_3O_4$@$Cu_2O$.

diffraction peaks (Fig. 2, c–g) which belong to the planes of a cubic phase of Cu crystals (PDF Card No. 04-0836). Quantitative analysis to determine the ratio of Cu/$Cu_2O$ was carried out using calibration curve (Fig. S1†) established by employing the peak intensities at 36.4° and 43.3° from the powder XRD spectra of the standard samples, mechanically mixed $Cu_2O$ with Cu at various ratios. For example, the ratios of Cu/$Cu_2O$ were estimated as 0.32 mol% and 1.01 mol% for $Fe_3O_4$@$Cu_2O$-5 and $Fe_3O_4$@$Cu_2O$–Cu-7 materials, respectively (Table S2†), which suggest that the content of Cu increased continuously as the reaction time increased.

As shown in Fig. 3a, $Fe_3O_4$ exhibited a rough surface of many irregular spherical structures with an average diameter of 385 nm that changed remarkably after the deposition of $Cu_2O$, Fig. 3b. The TEM images of the nanomaterial reveals much ordered structures of core–shell $Fe_3O_4$ which was surrounded by a layer of $Cu_2O$ nanospheres with an average thickness of

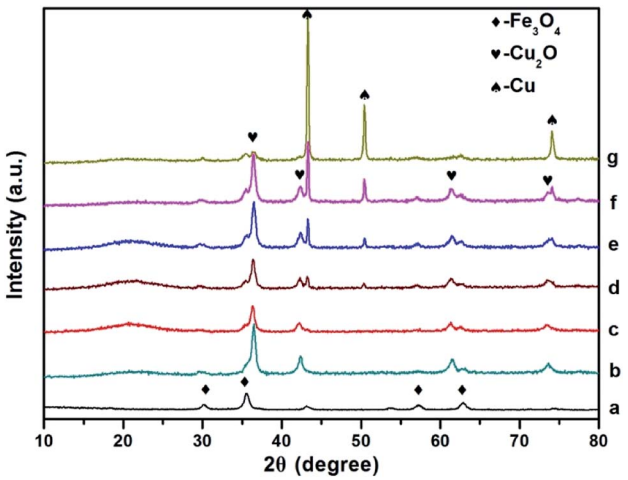


Fig. 2 Comparison of p-XRD spectra of $Fe_3O_4$ (a), $Fe_3O_4$@$Cu_2O$ ((b), 4 h), $Fe_3O_4$@$Cu_2O$–Cu nanomaterials ((c), 5 h; (d), 7 h; (e), 9 h; (f), 12 h) and $Fe_3O_4$@Cu ((g), 24 h).

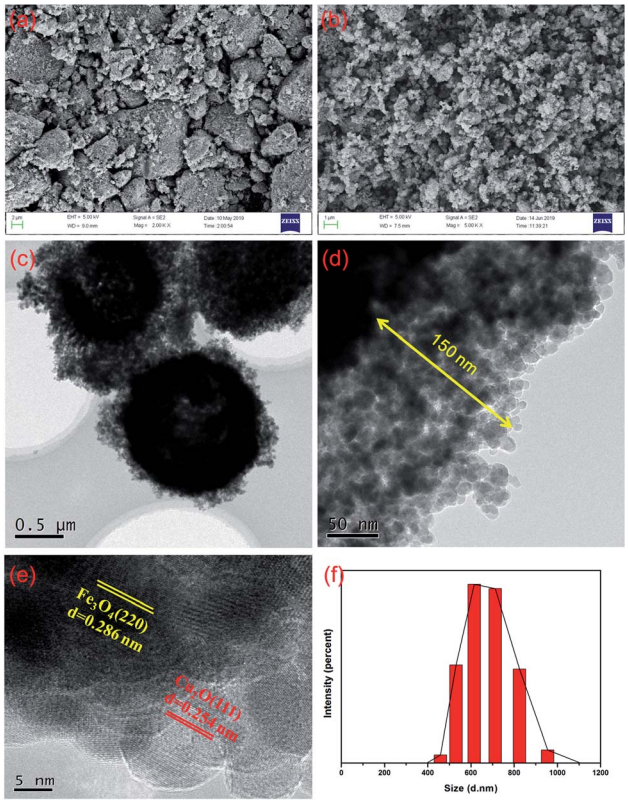


Fig. 3 SEM images of the as prepared $Fe_3O_4$ (a), core–shell $Fe_3O_4$@$Cu_2O$ (b), HR-TEM images of core–shell $Fe_3O_4$@$Cu_2O$ nanomaterial (c–e) and particle size distribution analysis for the core–shell $Fe_3O_4$@$Cu_2O$ nanomaterial (f).

150 nm, Fig. 3c and d. The HR-TEM images confirm the coexistence of $Fe_3O_4$ and $Cu_2O$ (Fig. 3e) in which the pattern corresponds to the planes of $Fe_3O_4$ (220) and $Cu_2O$ (111), respectively. Moreover, the core–shell $Fe_3O_4$@$Cu_2O$ nanomaterial has an average diameter of about 700 nm that can be evidenced from the particle size distribution shown in Fig. 3f. The average particle size of $Cu_2O$ in the nanospheres on the

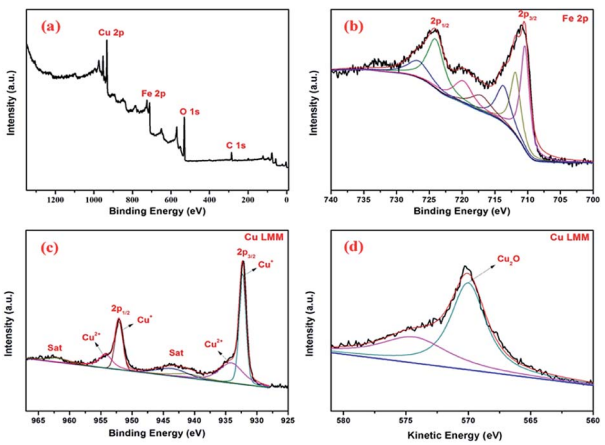


Fig. 4 XPS spectra of core shell $Fe_3O_4$@$Cu_2O$ nanomaterial: (a) survey spectrum; (b) Fe2p; (c) Cu2p; (d) Cu LMM Auger spectra.

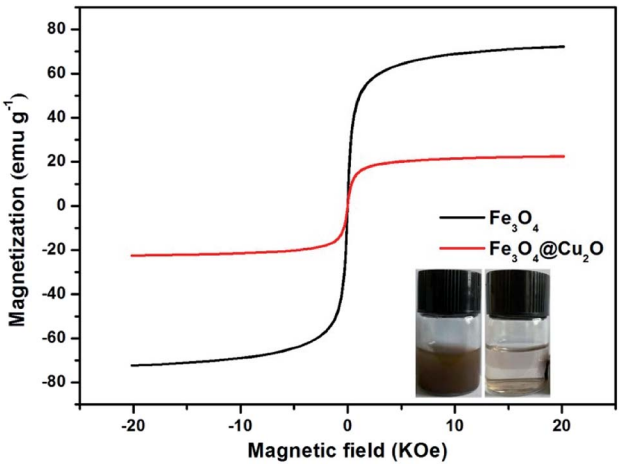


Fig. 5 Magnetization curves of $Fe_3O_4$ and $Fe_3O_4@Cu_2O$.

surface of the core–shell $Fe_3O_4$ was estimated as 16 nm by using Scherrer's formula.[42]

In order to reveal the oxidation states of the components and their interactions with each other, XPS study was carried out for $Fe_3O_4@Cu_2O$ (Fig. 4a–c). In Fig. 4a, the presence of Fe, Cu and O elements in the core–shell nanomaterials were confirmed. The two bands at 711.4 and 723.7 eV shown in Fig. 4b are assigned to $Fe2p_{3/2}$ and $Fe2p_{1/2}$, respectively, corresponding to $Fe^{2+}$ (FeO) and $Fe^{3+}$ ($Fe_2O_3$) peaks.[45] Intense core-level lines of Cu are shown as a Cu2p doublet ($Cu2p_{1/2}$ and $Cu2p_{3/2}$) between 920–970 eV (Fig. 4c). It shows two distinct peaks at 952.2 eV and 932.2 eV belonging to $Cu2p_{3/2}$ and $Cu2p_{1/2}$ of cuprous oxide, respectively.[48] There is a main peak at 532 eV assigned to the lattice O in cuprous oxide. The existence of cuprous oxide was also proved by Auger spectroscopy,[18] showing a sharp peak in Cu LMM triplet kinetic energy at 570.2 eV. Also, the characteristic peaks for the $Fe_3O_4$ and $Cu_2O$ in the over-reduced catalyst of $Fe_3O_4@Cu_2O$–Cu-7 was clearly coincident with the XPS data of $Fe_3O_4@Cu_2O$. In addition to those commonly observed peaks, a peak of weak intensity at 918.7 eV showed the existence of metallic Cu in the nanomaterial of $Fe_3O_4@Cu_2O$–Cu-7 (4).

The magnetic properties of the core–shell $Fe_3O_4@Cu_2O$ and its precursor was measured *via* the vibrating sample magnetometer (VSM). Fig. 5 shows the magnetic hysteresis curves of the $Fe_3O_4$ and core–shell $Fe_3O_4@Cu_2O$ nanomaterials, the saturation magnetization ($M_s$) values are 72.1 emu $g^{-1}$ and 22.5 emu $g^{-1}$, respectively. The low saturation magnetization value for $Fe_3O_4@Cu_2O$ was due to the increased content of the $Cu_2O$ nanospheres around the core–shell $Fe_3O_4$. This magnetic property allowed its easy separation in performing catalysis (Fig. 5, inset).

### 2.2 Catalytic activity on the aerobic oxidation of alcohols and its possible mechanism

The aerobic oxidation of benzyl alcohol was chosen as a probing reaction to investigate the catalytic efficiency of the core–shell nanomaterials. The optimization studies were carried out with various factors and the results are shown in Table 1. It was clear that either NMI alone or its combination with TEMPO without the core–shell materials did not make the reaction proceed (Table 1, entries 1–4). In presence of copper catalysts such as $Cu_2O$ and metallic copper along with NMI and TEMPO, the reaction proceeds well and afforded good yields (Table 1, entries 5 & 6). These results suggested that the copper catalysts played a major role as an active site in the present catalytic system. The magnetic $Fe_3O_4@Cu_2O$ catalyst along with NMI and TEMPO yielded quantitatively benzaldehyde as the sole product (Table 1, entry 7). Replacing *N*-methylimidazole (NMI) with 1-butyl and 1-*tert*-butylimidazoles did not affect substantially the yield but the

Table 1 Optimization of the reaction conditions for the aerobic oxidation of benzyl alcohol[a]

| Entry | Catalysts | TEMPO (mmol) | Ligand | Yield[b] (%) |
|---|---|---|---|---|
| 1 | — | — | NMI | — |
| | — | 0.25 | NMI | 1 |
| 3 | $Fe_3O_4$ | 0.25 | NMI | 1 |
| 4 | $Fe_3O_4@Cu_2O$ | 0.25 | — | 1 |
| 5 | Cu[c] | 0.25 | NMI | 94 |
| 6 | $Cu_2O$[d] | 0.25 | NMI | 90 |
| 7 | $Fe_3O_4@Cu_2O$ | 0.25 | NMI | 80[e]/>99 |
| 8 | $Fe_3O_4@Cu_2O$ | 0.25 | 1-Butyl imidazole | 99 |
| 9 | $Fe_3O_4@Cu_2O$ | 0.25 | 1-*tert*-Butyl imidazole | 96 |
| 10 | $Fe_3O_4@Cu_2O$–Cu-5 | 0.25 | NMI | 78[e]/>99 |
| 11 | $Fe_3O_4@Cu_2O$–Cu-7 | 0.25 | NMI | 68[e]/>99 |
| 12 | $Fe_3O_4@Cu_2O$–Cu-9 | 0.25 | NMI | 51[e]/>99 |
| 13 | $Fe_3O_4@Cu_2O$–Cu-12 | 0.25 | NMI | 46[e]/98 |
| 14 | $Fe_3O_4@Cu$ | 0.25 | NMI | 60[e]/91 |
| 15 | $Fe_3O_4@Cu_2O$[f] | 0.25 | NMI | >99 |

[a] Reaction conditions: alcohol (5 mmol), catalyst (15 mg), TEMPO (0.25 mmol), NMI (0.25 mmol), acetonitrile (5 mL), 25 °C, 18 h. For the sample coding, the suffix number *x* of the codes (entries 10–13) in $Fe_3O_4@Cu_2O$–Cu-*x* denotes the reaction time in the catalyst preparation. [b] Results by GC analysis. [c] 0.14 mmol. [d] 0.07 mmol. [e] Yield at 12 h. [f] At 82 °C for 12 h.

Table 2 Effect of solvents on the aerobic oxidation of benzyl alcohol[a]

| Entry | Solvent | Yield[b] (%) |
|---|---|---|
| 1 | $H_2O$ | 46 |
| 2 | DCM | 64 |
| 3 | DMF | 46 |
| 4 | DMSO | 21 |
| 5 | THF | 89 |
| 6 | Toluene | 86 |
| 7 | $CH_3CN$ | >99 |

[a] Reaction condition: alcohol (5 mmol), $Fe_3O_4$@$Cu_2O$ (15 mg), NMI (0.25 mmol), TEMPO (0.25 mmol), solvent (5 mL), 25 °C, 18 h. [b] Confirmed by GC analysis.

reaction rate slowed down (Table 1, entries 8 & 9). Compared to the $Fe_3O_4$@$Cu_2O$, the over-reduced catalysts of $Fe_3O_4$@$Cu_2O$–Cu with different contents of Cu showed essentially the same activities as $Fe_3O_4$@$Cu_2O$ (Table 1, entries 10–13). But in reaction rate, the presence of metallic copper made some differences. It seems that the increase in the ratio of metallic copper retarded the reaction at its initial stage although at the end of the reaction, the yield was not affected significantly. Further, the presence of the metal copper seems to enhance its robustness (*vide infra*). By increasing the temperature to 82 °C (Table 1, entry 15), the reaction rate was increased substantially in the initial stage and the reaction time can be shorted to 12 h (Fig. S3†).

In order to check the influence of a solvent on the catalysis, various protic and aprotic solvents were employed under similar conditions and the results are presented in Table 2. The conversion results are more favourable in less-polar solvents like Toluene, THF, DCM and $CH_3CN$ than polar solvents such as $H_2O$, DMF, and DMSO (Table 2, entries 1–7). Especially, in acetonitrile, the reaction proceeded well and afforded excellent yield (>99%), which agrees with what was observed in homogenous catalysis by $Cu^I$/NMI/TEMPO.[23] Based on these results, acetonitrile was employed as the solvent medium throughout the study.

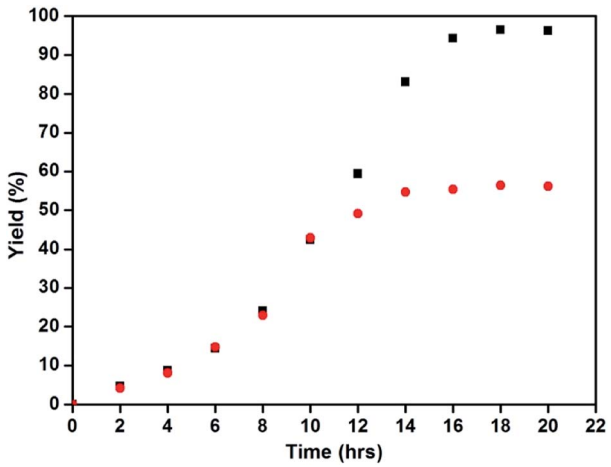


Fig. 6 Heterogeneity test of the $Fe_3O_4$@$Cu_2O$ catalyst (black: reaction proceeded as usual and red: reaction proceeded after $Fe_3O_4$@$Cu_2O$ was removed at 10 h).

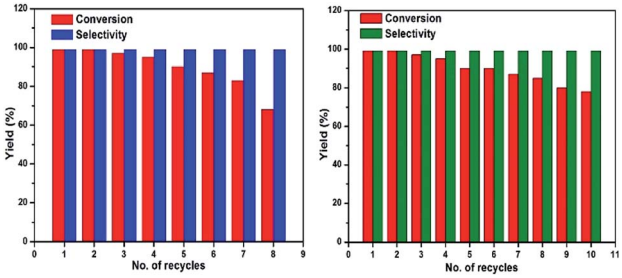


Fig. 7 Reusability of $Fe_3O_4$@$Cu_2O$ (left) and reusability of $Fe_3O_4$@$Cu_2O$–Cu-7 (right).

### 2.3 Heterogeneity and reusability of the catalysts

To check the heterogeneity of the catalyst, a set of normal reaction with optimized conditions were performed and the progress of the reaction was monitored for every 2 h. After 10 hours, the catalyst was removed from one of the experiments to allow the reaction to continue under the same conditions. At the end of the reaction, there was a slight increase in the yield without the presence of the catalyst, which was contributed to the bleached copper in the solution (Fig. 6).

The reusability of the catalyst was examined for the selective oxidation of benzyl alcohol. After the completion of reaction, the catalyst was separated by applying an external magnet and washed three times with acetonitrile, dried under vacuum at 60 °C for 12 hours before being used for next run under the same reaction conditions. Fig. 7 (left) shows the reusability of $Fe_3O_4$@$Cu_2O$ catalyst and it remained substantially active for over eight times. A slight decrease in catalytic activity after five repetitive runs was due to the loss of $Cu_2O$ *via* chemically bleaching. ICP analysis suggested that the copper being bleached into the solution accounted for 5.8% of the total copper content. As shown in Fig. 7 (right), the over-reduced catalysts, for example,

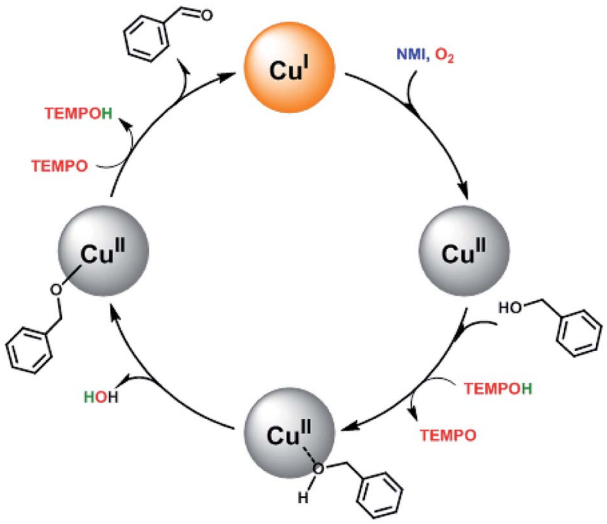


Scheme 2 A possible mechanism for the aerobic oxidation of benzylic alcohols catalyzed by the magnetic core–shell materials with both TEMPO and NMI as the co-catalysts.

$Fe_3O_4$@$Cu_2O$–Cu-7, exhibited much better stability. But at this stage, we do not understand how the co-existence of minimum amount of metallic copper in the catalyst could enhance its robustness. The p-XRD and XPS studies of the fresh and recycled catalysts of $Fe_3O_4$@$Cu_2O$–Cu-7 did not surrender much information on this matter (Fig. S4 and S5†).

Based on the previous reported literatures,[14,23] a simplified mechanism for this catalytic system was proposed in Scheme 2. First, $O_2$ is activated by Cu(I) and the metal site is oxidised to Cu(II). The involvement of NMI may enhance the reducing capability *via* coordination to the metal site and acts probably as a base as well. Then, the substrate is adsorbed on the surface at $Cu^{II}$ species, followed by deprotonation of the bound alcohol. This process is similar to the reported homogenous catalytic system, in which the hydroxyl group formed from the reduction of $O_2$ acted as an internal base and deprotonated readily the proton of the bound substrate to form alkoxide-bound adduct.[15,17,23] Finally, the abstraction of α-hydrogen from the substrate by TEMPO led to the desired carbonyl compound and regenerated Cu(I) species. Meanwhile, the production of TEMPOH could act as hydrogen source for next catalytic cycle supported by the evidence that the employment of TEMPOH, the reduced form of TEMPO, as the co-catalyst showed better catalytic activity than TEMPO in the catalysis at the initial stage (Fig. S6†).

This proposed mechanism was further confirmed by the results obtained from p-XRD and XPS studies of the recycled catalysts. The p-XRD data of the recycled catalysts (Fig. S2†) shown that the peak intensity of $Cu_2O$ was weakened, hence there were no characteristic peaks of CuO in the recycled catalysts (4th and 7th run). But the XPS spectra of the recycled catalysts of $Fe_3O_4$@$Cu_2O$ (4th & 7th recycle) revealed the formation of CuO by the presence of two additional peaks with binding energies of 934.20 eV and 954.14 eV respectively (Fig. 8, top left). It was further supported by the Cu LMM auger spectrum with the presence of additional peak at 568.5 eV for CuO along with $Cu_2O$ (Fig. 8, Top right).

In the O1s core level, there is an increase in peak areas of O–$Cu^{2+}$ and surface-oxygen were observed for consecutive runs due to the surface oxidation of cuprous oxide (Fig. 8, bottom left). Analogously, a slight increase in the binding energy of N1s was also observed with the formation of N–$Cu^{2+}$ at 400.7 eV in the

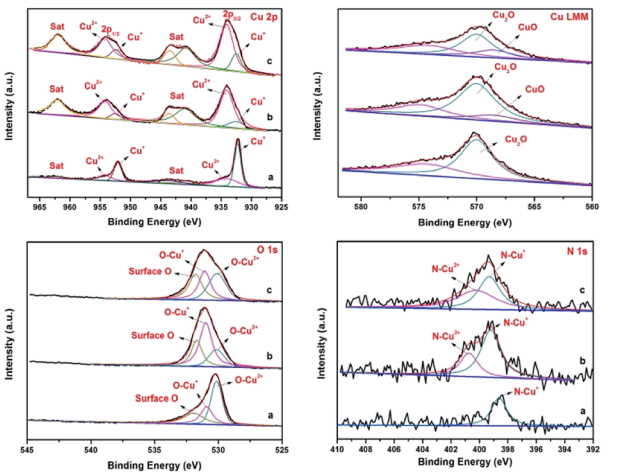


Fig. 8 Comparison of XPS spectra of fresh and recycled $Fe_3O_4$@$Cu_2O$ catalysts: Cu2p (Top left), Cu LMM (Top right), O1s (Bottom left) and N1s (Bottom right) spectrum; (a) fresh catalyst, (b) 4th recycling and (c) 7th recycling.

Table 3 Aerobic oxidation of various alcohols catalyzed by $Fe_3O_4$@$Cu_2O$ nanomaterial[a]

| Entry | Substrate | Product | Selectivity (%) | Yield[b] (%) |
|---|---|---|---|---|
| 1 | 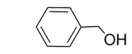 | 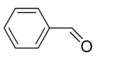 | >99 | >99 |
| 2 | 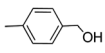 | 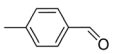 | >99 | >99 |
| 3 | 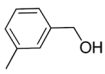 | 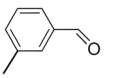 | >99 | 92 |
| 4 | 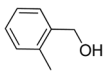 | 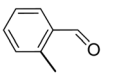 | >99 | 96 |
| 5 | 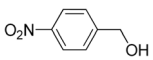 | 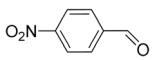 | >99 | >99 |
| 6 | 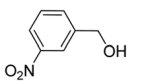 | 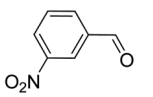 | >99 | >99 |
| 7 | 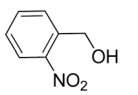 | 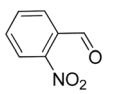 | >99 | >99 |
| 8 | 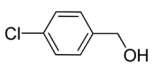 | 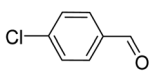 | >99 | >99 |
| 9 | 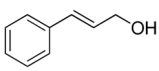 | 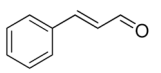 | >99 | >99 |
| 10 | 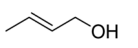 | 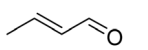 | >99 | >99 |
| 11 | 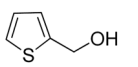 | 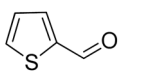 | >99 | >99 |
| 12 | 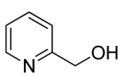 | 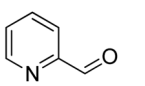 | >99 | 14 |
| 13 | 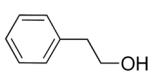 | 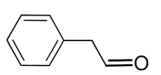 | 16.5 | 9 |
| 14 |  | 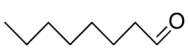 | >99 | 5 |
| 15 | 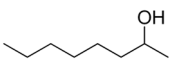 | 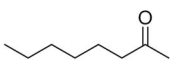 | >99 | 3 |
| 16 | 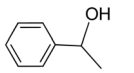 | 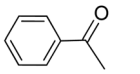 | — | — |

[a] Reaction conditions: alcohol (5 mmol), $Fe_3O_4$@$Cu_2O$ (15 mg), TEMPO (0.25 mmol, 39.1 mg), NMI (0.25 mmol, 20 mg), $CH_3CN$ (5 mL), 25 °C, 18 h. [b] Confirmed by GC-MS analysis.

Table 4 Comparison with the catalytic systems reported in the literatures for the oxidation of benzyl alcohols

| Entry | Reaction conditions | Selectivity (%) | Yield (%) | Catalyst recycle | Ref. |
|---|---|---|---|---|---|
| **1** | **$Fe_3O_4$@$Cu_2O$, NMI, TEMPO, air, 25 °C, 18 h** | **>99** | **99** | **Magnetisation** | **This work** |
| 2 | $Fe_2O_4$–Co, $H_2O_2$, 110 °C, 5 h | 100 | 99 | Magnetisation | 42 |
| 3 | $Fe_3O_4$/Cys–Pd, $O_2$, 55 °C, 1.5 h | >99 | 85 | Magnetisation | 43 |
| 4 | $Fe_3O_4$/MPA–PHEA-Cr, $O_2$, 45 °C, 4 h | 99 | 60 | Magnetisation | 44 |
| 5 | CuO–rectorite, TEMPO, $K_2CO_3$, $O_2$, 50 °C, 24 h | >99 | 85 | Centrifugation | 38 |
| 6 | Cu–$MnO_x$, TEMPO, $O_2$, 120 °C, 6 h | 98 | 98 | Centrifugation | 39 |
| 7 | $Cu_3(BTC)_2$, TEMPO, $Na_2CO_3$, $O_2$, 75 °C, 22 h | 98 | 89 | Centrifugation | 31 |
| 8 | Ru-kaolin, TBHP, $O_2$, 100 °C, 3 h | 100 | 97 | Centrifugation | 30 |

recycled catalysts (Fig. 8, bottom right). The XPS studies of the recycled $Fe_3O_4$@$Cu_2O$–Cu-7 also reveals the above same information except the formation of instable intermediate $Cu(OH)_2$ species (Fig. S7,† top right). In the O1s spectrum, the intensity of O–$Cu^+$ and O–$Cu^{2+}$ was slightly lower than that of surface oxygen (Fig. S7,† bottom left). Perhaps, the oxidation of metallic copper present in the catalyst might be a reason for the enhancement of reusability and robustness of the over-reduced $Fe_3O_4$@$Cu_2O$–Cu-7 catalyst.

### 2.4 Substrate scope

To explore the applicable scope of the catalysts, various alcoholic substrates were tested under the optimized reaction conditions and the results are summarized in Table 3. In most cases, selective oxidation of benzyl alcohols into corresponding aldehydes proceeded quantitatively with aldehydes as the sole products. Electron-donating groups like methyl-substituted benzyl alcohols showed slightly differentiated results among *para*-, *meta*- and *ortho*-positions (Table 3, entries 2–4), which could be contributed to both electronic and steric reasons. However, it is surprising that electron-withdrawing groups like chloro and nitro substituted benzyl alcohols did not show any negative effect on the reaction (Table 3, entries 5–8). In fact, on the contrary, it seems that the electron-withdrawing group promoted the catalysis. It is well known that during the conversion of an alcohol into its aldehyde, a number of steps are involved, for example, deprotonating the bound substrate before the first electron transfer and the abstraction of the hydrogen atom from the methylene group which accompanies the transfer of the second electron to complete the oxidation. These observations may imply that in the catalytic reaction, the deprotonation is one of the rate-determining steps and the abstraction of hydrogen atom from the methylene group is not, since electron-withdrawing group would increase the acidity of the substrate. For allylic alcohols, the catalyst showed also excellent efficiency (Table 3, entries 9 & 10). Furthermore, the catalyst was effective on some of the aerobic oxidation of heterocyclic alcohols (Table 3, entry 11). Interestingly, for pyridin-2-yl-methanol the activity dropped drastically (Table 3, entry 12). This may be due to that the nitrogen atom on the pyridyl group competed with the NMI for coordination which might block the catalytic sites and resulted in a very low yield, which agrees with what was observed in homogenous catalysis.[23] Finally, it must be said that its activity on aerobic oxidation of aliphatic alcohols and secondary alcohols was low (Table 3, entries 14–16).

Compared to those catalytic systems reported in the literatures (Table 4), the present catalytic system has the advantages, easy separation, functional group tolerance, using atmospheric air as the oxidant, operation at room temperature, good durability and reusability.

## 3. Conclusions

In summary, we have reported the preparation and characterisation of $Fe_3O_4$@$Cu_2O$ magnetic materials and its over-reduced analogues. Alongside with TEMPO and NMI additive, the magnetic materials showed excellent catalytic efficiency towards the aerobic oxidation of benzylic alcohols under ambient conditions. The electron-withdrawing groups seem to promote the reaction with no differentiation in their substituting position on the phenyl ring. On the contrary, the electron-donating groups such as methyl group did show subtle decrease in activity when the methyl group was at *ortho*- and *para*-positions. These observations may suggest that the deprotonation step in the catalysis might be important and be one of the rate-determining steps since an electron-withdrawing group would certainly increase the acidity of the alcohol and thus facilitate its deprotonation. In addition to its easy separation, the materials showed robustness in repetitive applications with no significant loss in activity. The over-reduced materials, $Fe_3O_4$@$Cu_2O$–Cu-7, showed even better durability. Further work has been undertaken to improve its catalytic activity for the aerobic oxidation of aliphatic alcohols and explore how the presence of metallic copper in the materials improved the robustness.

## 4. Experimental

### 4.1 Materials and instrumentation

All commercial reagents, substrates were purchased from Aldrich, Macklin or Aladdin and used as received without

 

further purification. The as-prepared core–shell $Fe_3O_4$@$Cu_2O$ nanomaterial and its precursors were characterized by different spectroscopic methods. IR (KBr) spectra were recorded on a Perkin-Elmer 781 spectrophotometer. X-ray diffraction (XRD) measurements were performed with a Philips powder diffractometer type PW 1373 goniometer. It was equipped with a graphite monochromator crystal. The X-ray wavelength was 1.5405 Å and the diffraction patterns were recorded in the $2\theta$ range (10–80) with scanning speed of $2^\circ$ $min^{-1}$. Morphology and particle dispersion was investigated by scanning electron microscopy (SEM) (Cam scan MV2300). The chemical composition of the as prepared nanomaterial was measured by EDS (Energy Dispersive X-ray Spectroscopy) performed in SEM. The shape and size of the $Fe_3O_4$@$Cu_2O$ nanomaterial were identified by transmission electron microscope (TEM) using a Philips EM208 microscope operating at an accelerating voltage of 90 kV. XPS analysis was used to investigate the oxidation states of elements by measuring the binding energy of that element. XPS experiments were performed with an Al KR monochromator X-ray source operating at 15 kV using Thermo Fisher Scientific, USA. During spectrum acquisition, the test chamber pressure is maintained above 10–6 mbar for using low-energy electrons to expel electron guns to neutralize possible surface roughness. Magnetic properties of the NPs were detected by a superconducting quantum interference device of vibrating sample magnetometer (SQUID, Quantum Design MPMS).

### 4.2 Synthesis of $Fe_3O_4$ nanomaterials

The magnetite nanomaterials ($Fe_3O_4$) were synthesized by the co-precipitation method according to the reported literature.[49] About 5.84 g of $FeCl_3 \cdot 6H_2O$ and 2.15 g of $FeCl_2 \cdot 4H_2O$ ($Fe^{3+} : Fe^{2+} = 2 : 1$) were dissolved in 100 mL of deionized water under $N_2$ atmosphere at 85 °C. Then, 10 mL of 25% $NH_4OH$ was added and stirred for 2 h. Now, the colour of the bulk solution turned to black, the precipitates were separated and washed several times with deionized water and ethanol using magnetic decantation. After that, $Fe_3O_4$ nanomaterials were treated with 0.1 M L-lysine solution for 30 min, which were then separated with a magnet and washed several times with deionized water and dried under vacuum at 60 °C for 10 h.

### 4.3 Synthesis of core–shell $Fe_3O_4$@$Cu_2O$ nanomaterials

The synthesis of core–shell $Fe_3O_4$@$Cu_2O$ nanomaterials was based on the reported literature method.[49] About 0.18 g of $Cu(NO_3)_2 \cdot 3H_2O$ was added to a mixture containing 17 mL of ethanol and 8.5 mL of ethylene glycol, followed by vigorous stirring. Then 25 mg of as-prepared magnetite was added to the above solution and sonicated for 30 min. After that, it was sealed in a Teflon-lined stainless-steel autoclave (100 mL capacity) and heated to 160 °C for 4 h. Then, the resultant solid was magnetically separated by using external magnet and washed three times with deionized water and ethanol to eliminate inorganic and organic impurities. Finally, the obtained core–shell $Fe_3O_4$@$Cu_2O$ nanomaterial was dried under vacuum at 60 °C for 5 h. The over-reduced materials were analogously prepared by prolonging the reaction time.

### 4.4 Aerobic oxidation of alcohols using core–shell $Fe_3O_4$@$Cu_2O$ nanomaterials

All reactions were carried out on a reaction tube (25 mL) in which benzyl alcohol (5 mmol), catalyst (15 mg), TEMPO (0.25 mmol), NMI (0.25 mmol) and acetonitrile (5 mL) were added respectively and stirred at room temperature. The aliquots of the reaction mixture were used for product analysis at regular interval by gas chromatic technique. The retention times for various compounds were determined by injecting pure compounds under identical GC conditions. Conversion of substrates was calculated from GC data and the oxidation products were identified from GC-MS results. At the end of the reaction, the catalyst was collected using an external magnet and reused for next run where applicable.

## Conflicts of interest

There are no conflicts to declare.

## Acknowledgements

The authors would like to thank the National Natural Science Foundation of China (Grant no. 21571083), the Natural Science Foundation of Zhejiang Province (Grant no. LY18B010007, LY19B010001), Science and Technology Program of Jiaxing (Grant No. 2018AY11003, 2018AY11010), the Government of Zhejiang Province (Qianjiang Professorship for XL) and Jiaxing University (Summit Program of Jiaxing University for Leading Talents) for supporting this work.

## Notes and references

1 E. I. Solomon, U. M. Sundaram and T. E. Machonkin, *Chem. Rev.*, 1996, **96**, 2563–2606.
2 J. P. Klinman, *Chem. Rev.*, 1996, **96**, 2541–2562.
3 M. M. Whittaker and J. W. Whittaker, *Biophys. J.*, 1993, **64**, 762–772.
4 E. T. T. Kumpulainen and A. M. P. Koskinen, *Chem.–Eur. J.*, 2009, **15**, 10901–10911.
5 C. Parmeggiani and F. Cardona, *Green Chem.*, 2012, **14**, 547–564.
6 M. E. Ali, M. M. Rahman, S. M. Sarkar and S. B. A. Hamid, *J. Nanomater.*, 2014, **2014**, 1–23.
7 R. Trammell, K. Rajabimoghadam and I. Garcia-Bosch, *Chem. Rev.*, 2019, **119**, 2954–3031.
8 P. Chaudhuri, M. Hess, U. Flörke and K. Wieghardt, *Angew. Chem., Int. Ed.*, 1998, **37**, 2217–2220.
9 M. Fabbrini, C. Galli, P. Gentili and D. Macchitella, *Tetrahedron Lett.*, 2001, **42**, 7551–7553.
10 P. Chaudhuri, M. Hess, T. Weyhermüller and K. Wieghardt, *Angew. Chem., Int. Ed.*, 1999, **38**, 1095–1098.
11 Y. Sasano, N. Kogure, S. Nagasawa, K. Kasabata and Y. Iwabuchi, *Org. Lett.*, 2018, **20**, 6104–6107.
12 G. Zhan, W. Zhong, Z. Wei, Z. Liu and X. Liu, *Dalton Trans.*, 2017, **46**, 8286–8297.

13 M. F. Semmelhack, C. R. Schmid, D. A. Cortes and C. S. Chou, *J. Am. Chem. Soc.*, 1984, **106**, 3374–3376.
14 R. A. Sheldon, I. W. C. E. Arends, G.-J. ten Brink and A. Dijksman, *Acc. Chem. Res.*, 2002, **35**, 774–781.
15 J. M. Hoover, B. L. Ryland and S. S. Stahl, *J. Am. Chem. Soc.*, 2013, **135**, 2357–2367.
16 B. L. Ryland and S. S. Stahl, *Angew. Chem., Int. Ed.*, 2014, **53**, 8824–8838.
17 J. M. Hoover, B. L. Ryland and S. S. Stahl, *ACS Catal.*, 2013, **3**, 2599–2605.
18 B. Chen, L. Wang and S. Gao, *ACS Catal.*, 2015, **5**, 5851–5876.
19 D. Zhai and S. Ma, *Org. Chem. Front.*, 2019, **6**, 3101–3106.
20 L. Marais and A. J. Swarts, *Catalysts*, 2019, **9**, 395–422.
21 M. M. Hossain and S.-G. Shyu, *Adv. Synth. Catal.*, 2010, **352**, 3061–3068.
22 A. Ochen, R. Whitten, H. E. Aylott, K. Ruffell, G. D. Williams, F. Slater, A. Roberts, P. Evans, J. E. Steves and M. J. Sanganee, *Organometallics*, 2019, **38**, 176–184.
23 Z. Liu, Z. Shen, N. Zhang, W. Zhong and X. Liu, *Catal. Lett.*, 2018, **148**, 2709–2718.
24 Z. Guo, B. Liu, Q. Zhang, W. Deng, Y. Wang and Y. Yang, *Chem. Soc. Rev.*, 2014, **43**, 3480–3524.
25 Y.-Z. Chen, R. Zhang, L. Jiao and H.-L. Jiang, *Coord. Chem. Rev.*, 2018, **362**, 1–23.
26 J. Habermann, S. V. Ley and J. S. Scott, *J. Chem. Soc., Perkin Trans. 1*, 1999, **1**, 1253–1256.
27 A. Bleloch, B. F. G. Johnson, S. V. Ley, A. J. Price, D. S. Shephard and A. W. Thomas, *Chem. Commun.*, 1999, 1907–1908.
28 L. Chen, T. Feng, P. Wang, Z. Chen, R. Yan, B. Liao and Y. Xiang, *Appl. Catal., A*, 2016, **523**, 304–311.
29 Y. Li, Y. Gao and C. Yang, *Chem. Commun.*, 2015, **51**, 7721–7724.
30 B. Zadam, D. Obaid, A. Mayoufi, P. Beaunier, F. Launay and F. Z. El Berrichi, *Res. Chem. Intermed.*, 2019, **45**, 1281–1293.
31 A. Dhakshinamoorthy, M. Alvaro and H. Garcia, *ACS Catal.*, 2011, **1**, 48–53.
32 S.-C. Chen, S.-N. Lu, F. Tian, N. Li, H.-Y. Qian, A.-J. Cui, M.-Y. He and Q. Chen, *Catal. Commun.*, 2017, **95**, 6–11.
33 X. Zhou and H. Ji, *Chin. J. Catal.*, 2012, **33**, 1906–1912.
34 G. Zhao, F. Yang, Z. Chen, Q. Liu, Y. Ji, Y. Zhang, Z. Niu, J. Mao, X. Bao, P. Hu and Y. Li, *Nat. Commun.*, 2017, **8**, 14039.
35 R. Poreddy, C. Engelbrekt and A. Riisager, *Catal. Sci. Technol.*, 2015, **5**, 2467–2477.
36 J. Albadi, A. Alihoseinzadeh and A. Mansournezhad, *Synth. Commun.*, 2015, **45**, 877–885.
37 H. Wang, W. Fan, Y. He, J. Wang, J. N. Kondo and T. Tatsumi, *J. Catal.*, 2013, **299**, 10–19.
38 W. Liu, J. Yang and J. Cai, *Res. Chem. Intermed.*, 2019, **45**, 549–561.
39 R. Ali, K. Nour, A. Al-warthan and M. R. H. Siddiqui, *Arabian J. Chem.*, 2015, **8**, 512–517.
40 J. Fan, Y. Dai, Y. Li, N. Zheng, J. Guo, X. Yan and G. D. Stucky, *J. Am. Chem. Soc.*, 2009, **131**, 15568–15569.
41 Q. Zhang, X. Yang and J. Guan, *ACS Appl. Nano Mater.*, 2019, **2**, 4681–4697.
42 M. Nasrollahzadeh, M. Bagherzadeh and H. Karimi, *J. Colloid Interface Sci.*, 2016, **465**, 271–278.
43 F. Zamani and S. M. Hosseini, *Catal. Commun.*, 2014, **43**, 164–168.
44 F. Zamani, S. M. Hosseini and S. Kianpour, *Dalton Trans.*, 2014, **43**, 3618–3625.
45 L. Geng, B. Zheng, X. Wang, W. Zhang, S. Wu, M. Jia, W. Yan and G. Liu, *ChemCatChem*, 2016, **8**, 805–811.
46 R. Azuma, S. Nakamichi, J. Kimura, H. Yano, H. Kawasaki, T. Suzuki, R. Kondo, Y. Kanda, K.-i. Shimizu, K. Kato and Y. Obora, *ChemCatChem*, 2018, **10**, 2378–2382.
47 M. Tang, S. Zhang, X. Li, X. Pang and H. Qiu, *Mater. Chem. Phys.*, 2014, **148**, 639–647.
48 Z.-P. Li, Y.-Q. Wen, J.-P. Shang, M.-X. Wu, L.-F. Wang and Y. Guo, *Chin. Chem. Lett.*, 2014, **25**, 287–291.
49 A. B. Raut and B. M. Bhanage, *ChemistrySelect*, 2017, **2**, 10055–10060.

 